

# We are IntechOpen, the world's leading publisher of Open Access books Built by scientists, for scientists

6,100

Open access books available

167,000

International authors and editors

185M

Downloads

Our authors are among the

154

Countries delivered to

TOP 1%

most cited scientists

12.2%

Contributors from top 500 universities



WEB OF SCIENCE™

Selection of our books indexed in the Book Citation Index  
in Web of Science™ Core Collection (BKCI)

Interested in publishing with us?  
Contact [book.department@intechopen.com](mailto:book.department@intechopen.com)

Numbers displayed above are based on latest data collected.  
For more information visit [www.intechopen.com](http://www.intechopen.com)



## Chapter

# Plasma Nitriding-Assisted 3D Printing for Die Technology in Digital Micro-Manufacturing

*Tatsuhiko Aizawa, Tomomi Shiratori and Yohei Suzuki*

## Abstract

A plasma nitriding-assisted 3D printing method was developed to build up the micro-punch and micro-die systems. Two dimensional punch head and core-die cavity geometries were ink-jet printed or screen-printed onto the AISI316 and SKD11 tool substrate surfaces in following their two-dimensional computer-aided design (CAD) data. The low-temperature plasma nitriding process was utilized to make nitrogen supersaturation only into the unprinted substrates. The sand-blasting and chemical etching were utilized to mechanically or chemically remove the printed parts from punch and die substrate. As sand-blasted and chemically etched AISI316 and SKD11 punches and core-dies were simply finished and used as a die set for micro-embossing, micro-piercing and micro-punching processes. In particular, a micro-pump was selected as a miniature mechanical element. Its 3D CAD geometry was sliced to 2D CAD data for each functional AISI304 stainless steel sheet. A pair of punch and die for each 2D CAD geometry for constituent sheet was prepared by the plasma nitriding-assisted 3D printing. Each sheet was punched out by using this set of punch and die to functionalize each sheet unit in correspondence to the sliced CAD data. These constituent sheets were assembled and joined to a structural unit of micro-pump.

**Keywords:** micro-parts, micro-tools, 3D plasma printing, 2D screen printing, micro-embossing, micro-piercing, surface activation, low-temperature joining, micro-pump

## 1. Introduction

The additive manufacturing with the use of three-dimensional (3D) printing method has grown up as a fundamental scheme to fabricate the polymer, the ceramic, and the metal products with complex geometry [1]. Its feedstock is usually a powder or a particle with the specially designed alloying elements [2]. These powder materials are melt by application of high power supply via the lasers [3], the electron beams [4], and the plasma torch [5]. Since these materials are melt, solidified, and sintered pointwise within the power hot spot, the resolution in geometry is determined by the scanning in power supply and the hot spot size [6]. The total configuration of product in geometry is roughly built up by solidification and sintering processes in these 3D printing; the finishing step is still necessary to satisfy the design requirement [7].

Without the high-resolution techniques and material selection, a miniature product with strict requirement in dimension is difficult to be yielded by 3D printing, since its resolution is much lower than the product dimensional requirement. It is also unsuitable to mass production of parts and devices with complex geometry, e. g. micro-element for micro-electric mechanical system (MEMS), micro-parts and device for medical applications, mm-sized punch and die, and miniature mechanical parts with high-quality proof.

Let us change the normal feedstock for additive manufacturing to the metal and plastic foils, films, sheets, and plates. Most of them have been utilized as a feedstock of metal forming and plastic product processing with sufficient proof of strength and ductility. In addition, relatively wider material selection is available in this new additive manufacturing with the use of them. **Figure 1** illustrates the candidate scheme of additive micro-manufacturing to build up a micro-pump [8]. The three-dimensional CAD model of the micro-pump is sliced into a constituent two-dimensional model with each mechanical function. Except for the PZT unit to drive the micro-pump, its main unit is divided into an assembly of a grid, a shield, the reservoir plate, two diaphragm plates and valve plates, and an end plate. The metallic sheets and plates are prepared as a starting material with the suitable thickness to each constituent part of micro-pump unit. If the punch and die sets are simply prepared with sufficient accuracy in dimensions, each part is yielded even in mass production by blanking, punching, embossing, and piercing these plates as a feedstock.

In the normal die technology [9], the grinding, polishing, and machining processes are utilized to fabricate the punches and dies. In micro-manufacturing of punches and dies, the sub-mm and  $\mu\text{m}$ -ordered milling tools must be prepared to shape the miniature die substrates. In addition, lots of duration for preparation of Computer-Aided Machining (CAD) data and actual operations is needed only to fabricate a single punch even with the microtextures in  $10\ \mu\text{m}$  to  $100\ \mu\text{m}$  orders. When using the austenitic stainless steels or tool steels as a die substrate, the surface treatment is also necessary to strengthen and harden the punch under the severe dry stamping and

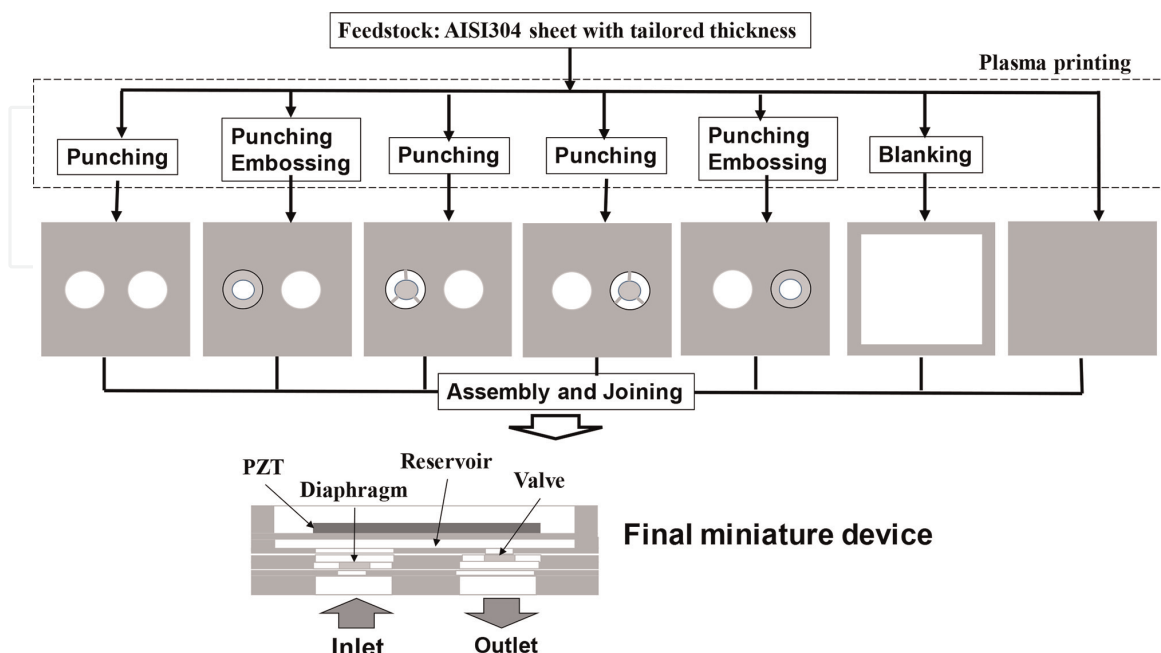


**Figure 1.** Advanced additive micro-manufacturing from the foils, films, sheets, and plates as a feed stock to fabricate a metallic miniature product.

forging conditions. Hence, it is difficult or nearly impossible to prepare a set of punch and die for blanking, punching, and embossing processes to yield the constituent sheets in correspondence to the sliced data of product CAD data.

The plasma nitriding-assisted 3D printing [10] provides a solution to the above issue of difficulty in the die technology. The positive micro-pattern to the sliced 2D product model is printed onto the die surface. Its unprinted parts are selectively hardened by plasma processing to transform the unprinted parts to the significantly hardened ones in the die substrate. The mechanical and chemical processes are utilized to selectively remove the printed and unhardened parts from the substrate. The punch and die are directly built up to have the designed punch head and die cavity for embossing, piercing, blanking, and punching the feedstock sheets and plates to each constituent element in **Figure 1**.

In the present chapter, this new additive micro-manufacturing is proposed to fabricate the mm-/sub-mm-ordered mechanical sheet parts with the sliced 2D CAD data of 3D product model by embossing, piercing, and punching processes and to assemble and join them to a miniature mechanical unit and device. The plasma nitriding-assisted 3D printing method is utilized as the first step to fabricate the punch and die pair with its complex head and core geometry from the sliced 2D CAD of product model. This approach has three merits as a die technology: 1) high surface hardness for long tool life in stamping and forging, 2) flexible and short-time response to 2D CAD, and 3) dimensional accuracy in geometry enough to be used in fabrication of products. Since the austenitic stainless steel and titanium sheets are selected as a feedstock, this high hardness leads to prolongation of punch and die lives in practical stamping and forging operations. The tailored complex geometries directly reflect on the punch head and core-die cavity shapes in much shorter duration than needed in the conventional die technology. Owing to the autonomous dimensional accuracy in the plasma printing, the 3D-printed punch and die is used after a bit duration in the finishing step.

First, the plasma nitriding-assisted 3D printing procedure is explained in the procedure from the CAD of cross-meshing pattern to build up the hardened punch with meshing-textured head. In second, the copper substrate for the plastic packaging of semiconductors is precisely stamped to have microgroove loops by using the micro-textured punch after optimum geometry design to minimize the thermal stresses under the thermal loading in usage of the mold packages. Owing to this optimized microgrooves, the leak proof is certified in 100%. AISI304 sheets are pierced to have a micro-valve unit by using the plasma-printed punch and die. A constituent sheet is yielded when starting from the sliced 2D geometry of the micro-pump model. An electrical steel sheet is also blanked to have a T-shaped motor core unit by using the simultaneously plasma-printed punch and die. High burnished surface area ratio is attained even in the sheared surface by using the as-blasted punch and die. Finally, a micro-pump unit is produced in trial after the scheme in **Figure 1**. The pierced AISI304 constituent sheets by the plasma-printed punch and die are assembled and joined to a micro-pump unit.

## **2. Plasma nitriding-assisted 3D printing**

### **2.1 Two-dimensional patterning and texturing**

This 3D printing starts from drawing the two-dimensional model after CAD data onto the tool surfaces as shown in **Figure 2a**. This printed pattern works as a mask to

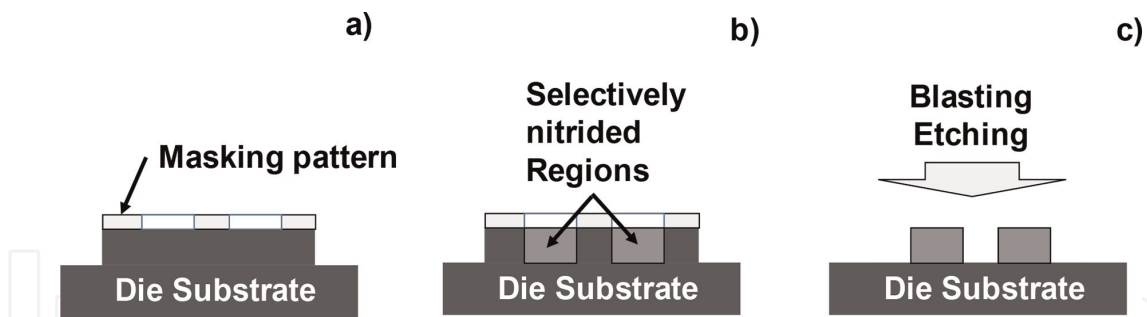


**Figure 2.** A normal plasma nitriding-assisted 3D printing procedure. a) Patterning the 2D model of CAD data onto the die surfaces, b) plasma nitriding the unmasked die, and c) removing mechanically, or, chemically etching the printed parts to leave the 3D-shaped tools.

prevent the printed tool surface from plasma nitriding as shown in **Figure 2b**. The unprinted parts of tool are selectively nitrogen-supersaturated to their specified depth. Due to their high nitrogen contents, they have selectively much higher hardness and corrosion toughness than the printed tool parts. Through mechanical removal and chemical etching in **Figure 2c**, the printed parts are cut off to leave the designed three-dimensional tool and product configurations in adaptive to the original 2D surface by CAD.

## 2.2 Two-dimensional printing of CAD data onto tools

Several methods are available to draw 2D CAD data onto the tool surfaces, e.g. masking [11], inkjet printing [12], screen printing [13], lithography [14], and short-pulse laser machining [15]. As shown in **Figure 3a**, the masking plate is first prepared and fixed onto the tool surface. No actual printing process is necessary; its spatial resolution is predetermined by the dimensional accuracy of masking plate. The inkjet printing is feasible to draw 2D CAD data onto the flat and curved tool surfaces as depicted in **Figure 3b**. A wider tool surface can be printed. Its resolution is also limited

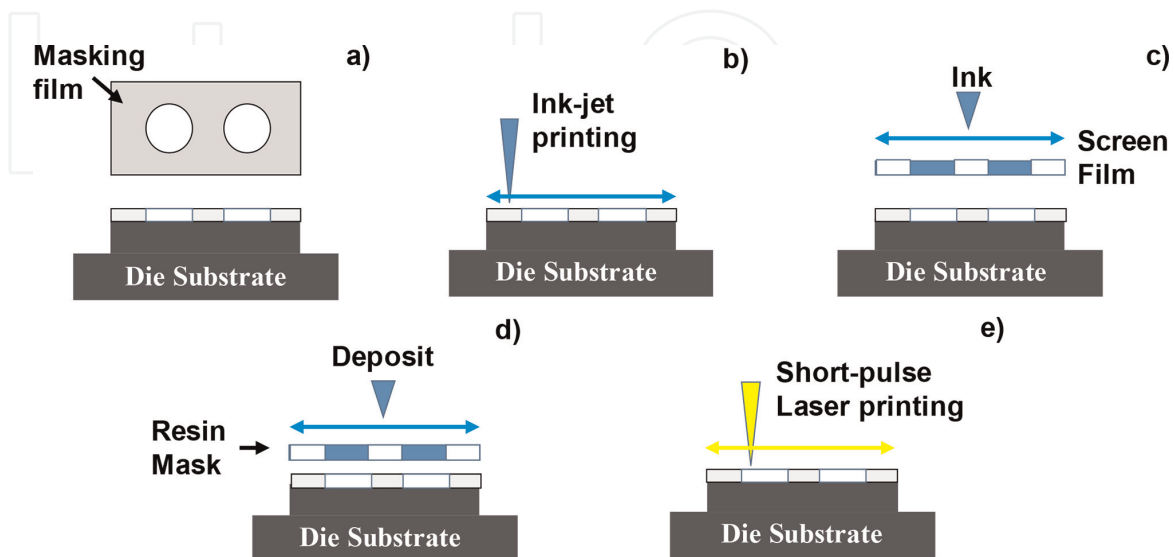


**Figure 3.** Five methods to pattern the 2D model of tools onto the die substrate surface. a) Masking, b) inkjet printing, c) screen printing, d) lithography, and e) laser printing.

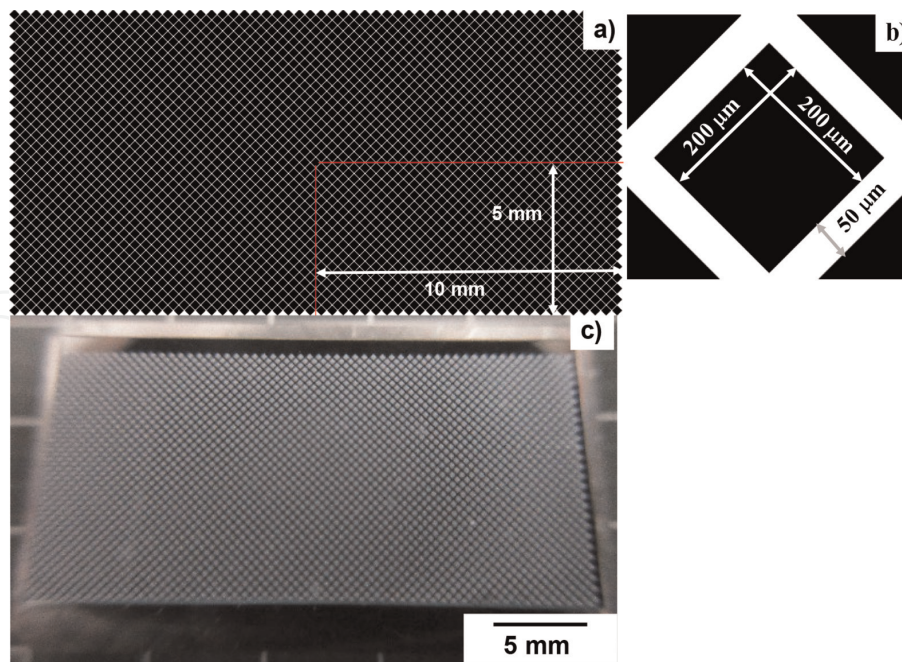


**Figure 4.** Screen printing of the meshing line pattern onto AISI316 die. a) Screen film with meshing pattern, b) its unit cell, and c) printed micro-pattern onto the die surface.

by the inner diameter of nozzle. The viscosity of ink influences on the accuracy in dispensing.

The positive pattern to original CAD data is formed onto the screen as shown in **Figure 3c**. In this screen printing, its resolution is determined by the meshing technique in the preparation of screen films. The lithography is a powerful tool to draw any patterns with higher resolution in dimension as depicted in **Figure 3d**. The trade-balancing must be taken into account between the dimensional accuracy in CAD and the cost in usage of lithography system. The short-pulse laser machining also provides a method to make fine drawing onto the thin sacrifice film on the tool surface as depicted in **Figure 3e**. Its spatial resolution is functional in the laser frequency, the laser pulse control, and the film thickness. The original CAD data are directly transformed into CAM data for laser machining to print the complex geometry in short duration.

Let us use the screen printing method to draw a micro-pattern onto AISI316 die surface with the area of 10 mm x 20 mm [16, 17]. A screen film was prepared in corresponding to the meshing pattern in 2D CAD, as depicted in **Figure 4a**. The ink penetrates through the black squares to leave the meshing lines unprinted. Its unit cell is depicted in **Figure 4b**; the line width is 50 μm and its pitch is 250 μm. **Figure 4c** shows the square pattern, printed onto the AISI316 die surface.

### 2.3 Nitrogen supersaturation into unprinted parts

The plasma nitriding has been widely utilized as a typical surface treatment of various steels and high chromium alloys as surveyed in [18]. Most of the commercial nitriding processes, so-called by the ion nitriding (DC nitriding) and the radical nitriding (DC pulse nitriding), were utilized to harden the steel die materials by fine nitride precipitate formation in the nitrided layer [19]. After [20], the surface hardness increased above 1000 HV in the DC-plasma-nitrided Fe-19Cr alloy at 773 K for

57.6 ks. This inner nitriding process at high holding temperature is governed by the nitrogen diffusion process as analyzed in [20–22]. Hence, high holding temperature is necessary to sustain the nitrogen diffusion and synthesis of chromium nitride (CrN) by  $\text{Cr} + \text{N} \rightarrow \text{CrN}$  during the plasma nitriding. On the other hand, the stainless steels as well as tool steels were nitrogen-supersaturated by the plasma nitriding at 673 K without nitride precipitation reactions [23–25]. The most different features from the high-temperature plasma nitriding processes in the above are as follows: 1) surface hardness increases over 2000 HV, 2) microstructure in the nitrided layer is refined to have very fine two-phase granular structure, 3) nitrogen solute distributes uniformly and homogeneously in the nitrided layer with the average content of 4 mass%, and 4) nitrogen supersaturation accompanies with the significant lattice expansion. In addition, the nitrided layer thickness turns to be more than 50  $\mu\text{m}$  after plasma nitriding at 673 K for 14.4 ks. This inner nitriding process at low holding temperature is not only governed by the nitrogen diffusion process but also controlled by the plastic straining. After [26, 27], the mismatched strains between the un-nitrided and nitrided zones are induced by the lattice expansion in the nitrogen supersaturation process. Most of nitrogen solute diffuse through the plastically strained zone boundaries so that the high nitrogen content is preserved in all the nitrided layer.

When using the printed pattern as a mask in this low-temperature plasma nitriding, the unprinted parts are only nitrogen-supersaturated to have higher hardness than 1400 HV and more nitrogen solute content than 4 mass% in average. Let us prove this selective nitrogen supersaturation process by plasma nitriding the printed AISI316 die in **Figure 4** at 673 K for 14.4 ks. As shown in **Figure 5a**, the square unit cell printed on the die remains the same as shown in **Figure 4b**, although the meshing line edges and corners became dull. **Figure 5b** depicts the nitrogen solute distribution by the SEM (scanning electron microscopy)–EDX (electron-dispersive X-ray spectroscopy) analysis. The nitrogen solute is only present in the unprinted regions but not in the printed regions. This proves that unprinted regions are selectively nitrogen-supersaturated.

## 2.4 Mechanical removal and chemical etching

The nitrided or unmasked regions have much higher hardness than the hardness of shooting media in the dry sandblasting. In addition, their corrosion toughness is much improved never to be in pitting corrosion by using the normal etchant. This difference in hardness and corrosion toughness between the nitrided and masked regions drives the selective removal of masked regions from the die substrate by sandblasting or by chemical etching processes [28, 29].

The nitrided AISI316 die in **Figure 5** was subjected to sandblasting. The silica particles with the diameter of 30  $\mu\text{m}$  and the hardness of 700 HV were used as a shooting medium for sandblasting. **Figure 6** depicts SEM image on the AISI316 die surface after slightly sandblasting for 300 s. The masked square regions in **Figures 4c** and **5** were selectively dug; the nitrided regions became a mesh-textured punch head. To be noticed, the original 2D boundaries between the nitrided and masked regions changed to the side surfaces of mesh-textured punch. This proves that nitrogen supersaturation and diffusion processes advances in straight way from the surface to the depth of die substrate to form the selectively hardened zones in correspondence to the mesh textures.

**Figure 7** shows an overview on the sandblasted AISI316 die. The whole die surface is modified to a mesh-textured punch head. This proves that mechanical removal of masked region advanced homogeneously so that the mesh-textured punch head has a uniform height with lower maximum surface roughness than 0.6  $\mu\text{m}$  [30].

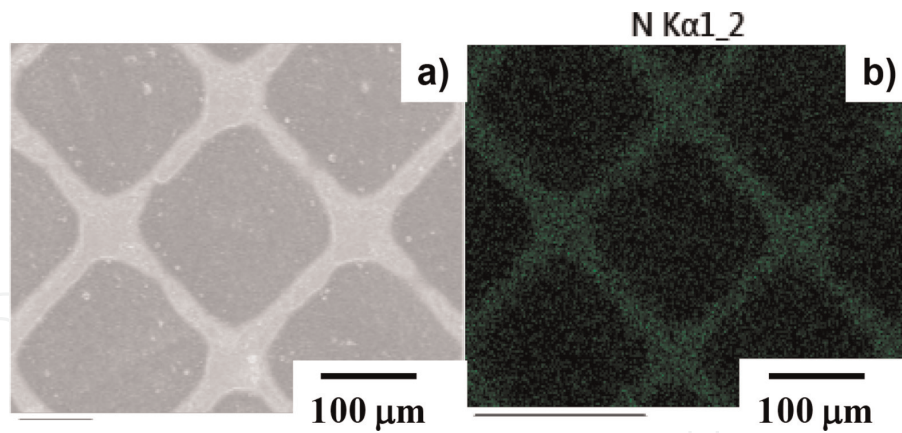


**Figure 5.** Meshing pattern-printed on the AISI316 die surface. a) SEM image on the meshing pattern, and b) nitrogen solute distribution on the AISI316 die surface.

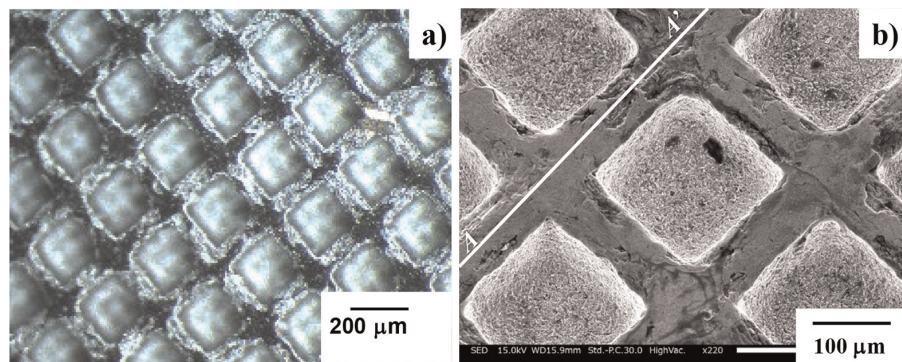


**Figure 6.** AISI316 die surface after sandblasting. a) SEM image in low magnification, and b) SEM image on high magnification.

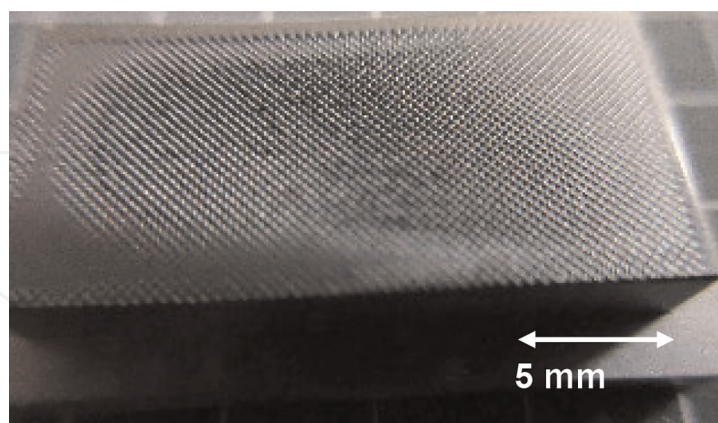


**Figure 7.** AISI316 die with the mesh-textured heads.

## 2.5 Dimensional measurement and characterization

Three-dimensional surface profiling system was utilized to measure the cross-sectional profile of mesh-textured die surface along the path in **Figure 8a**. As shown in **Figure 8b**, the clearance between adjacent nitrided pillars was uniformly formed to have constant depth and width in 80 μm and 250 μm, respectively. Each pillar has the same height and width of 80 μm and 40 μm, respectively.



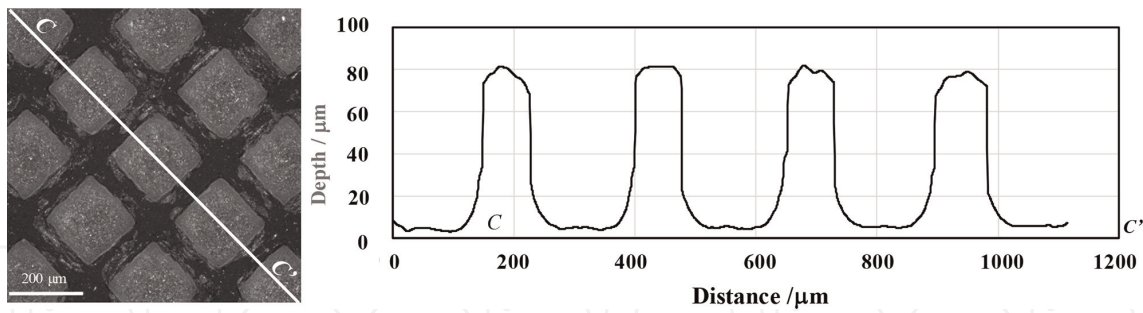


**Figure 8.** Three-dimensional die surface profile. a) SEM image on the measurement path, and b) cross-sectional view of mesh-textured die surface.

### 3. 3D printing of complex-shaped embossing punch for electronic packaging

The normal 3D printing has little means to deal with the multi-material product except for alloyed powders. In the semiconductor packaging, especially in the high-frequency GaN multi-chip packaging, the copper substrate must be strictly joined to a packaging plastic mold with sufficient robustness and tightness against the thermal transient loading [31–33]. The microgroove array to be dug into the copper substrate is first designed to reduce the thermal stresses in the substrate under the joined state to plastic mold. The tailored microgroove design is transformed into the embossing punch by using the 3D printing procedure in second. Fine coining system is utilized to form the microgroove array by embossing the 3D-printed punch. This copper substrate is mechanically joined with the plastic mold for packaging. These packages are subjected to thermal transient loading test for tightness proof in the actual thermal transients.

#### 3.1 Topological design on the microgroove array in the mold packaging

The high-power and high-frequency semiconductor unit with alignment of several gallium nitride (GaN) chips is packaged by joining the copper substrate with the plastic mold. As illustrated in **Figure 9**, both are mechanically joined through the microgrooves in the inside of copper substrate. Considering that thermal stresses are induced into the substrate during the thermal transient loading in operation, the topology of microgrooves must be optimized to reduce the thermal stress level in the inside and outside of joined area.

When using the simple linear loops of microgrooves, the thermal stress is enhanced to be high even in the inside and outside of joined interface to make

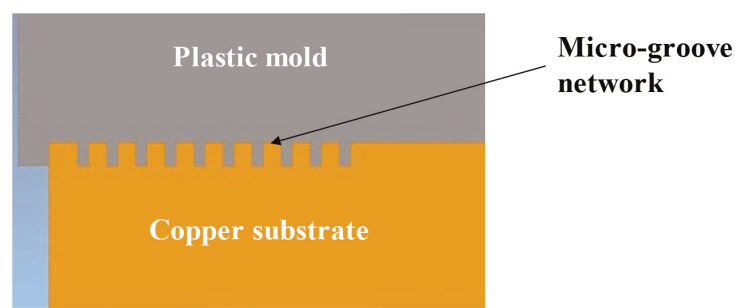


**Figure 9.** A schematic view on the cross section of copper-plastic mold package.

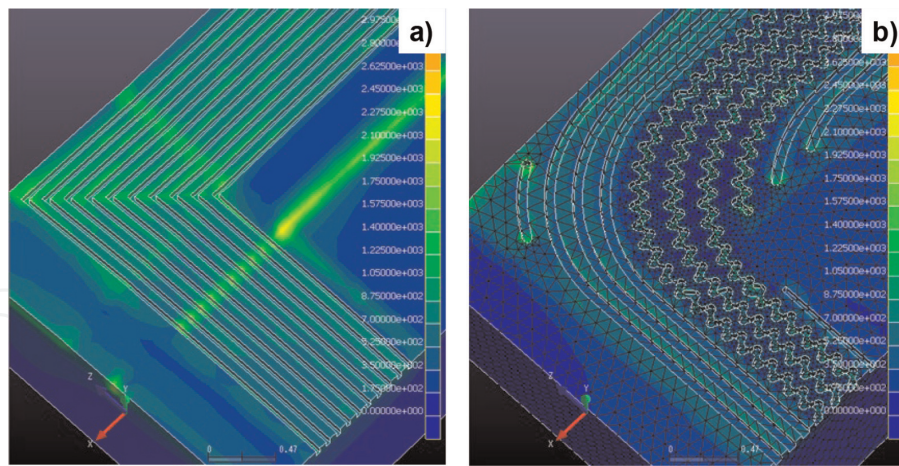


**Figure 10.** Comparison of the thermal stress distribution between the normal microgrooved package and the optimally tailored package.

distortion of chips and gold pins. This simple topology in **Figure 10a** is redesigned to a new configuration with continuous and discontinuous loops. As shown in **Figure 10b**, no significant stresses are observed both in the outside and inside of jointed interface. The continuous loops prevent the inside area from high thermal stress state; the discontinuous loops at the four corners of substrate preserve the low stress state even at the edges of substrate.

### 3.2 3D printing procedure

This tailored topology of microgrooves is cut in by using the plasma nitriding-assisted 3D printing procedure. After the general scheme in **Figure 2**, the screen film was prepared to print the two-dimensional CAD data of microgrooves onto the AISI316 die. **Figure 11a** depicts the 1/4 corner of screen-printed CAD data on the die. Two discontinuous loops (A and B) are placed at each corner of die in addition to three families of continuous loops {(C, D), (E, F, G), (H, K)} from the outside to the inside of die. As explained in the session 2, the black area in **Figure 11a** corresponds to a screen-printed mask and the white lines are left as an unprinted area. **Figure 11b** shows the SEM image on the die surface just after nitriding. As already demonstrated in **Figure 5**, the nitrogen solutes are supersaturated only into these discontinuous lines (A', B') and three continuous loops {(C', D'), (E', F', G'), (H', K')} in **Figure 11c**.

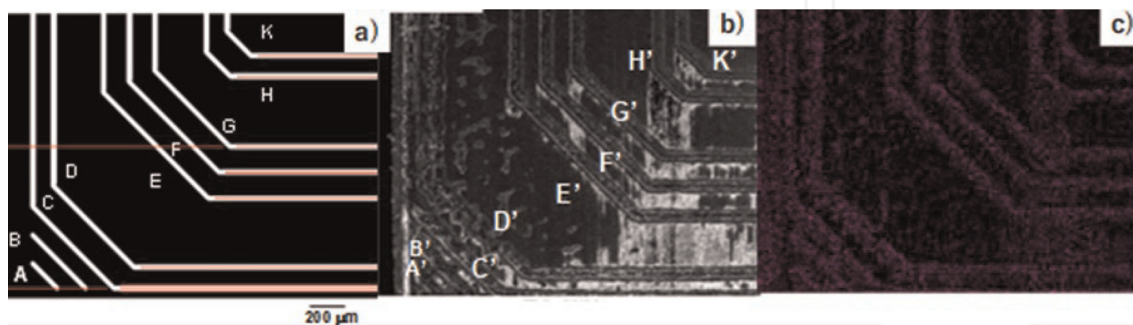


**Figure 11.** Plasma nitriding-assisted 3D printing from CAD data on the optimum microgroove topology to the 3D-printed embossing punch. a) Original topology design on the screen film, b) SEM image on the AISI316 die after nitriding, and c) nitrogen element mapping on the die surface.

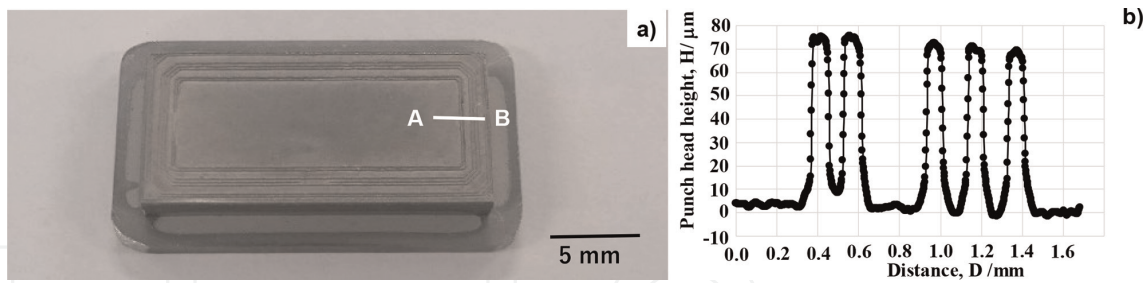


**Figure 12.** A plasma-printed AISI316 punch for embossing. a) Overview of the embossing punch, and b) its cross-sectional profile along A–B.

This also proves that the original tailored topology design is transformed to the nitrogen-supersaturated lines.

### 3.3 Fabrication of embossing punch with the tailored topology

The sandblasting was utilized to mechanically remove the printed regions from the die substrate in correspondence to **Figures 6–8** in the Section 2. **Figure 12a** depicts the AISI316 die after sandblasting for 300 s. The discontinuous loop heads and three families of continuous loop heads are automatically formed by the 3D printing as depicted in **Figure 12a**. Let us investigate the height profile of continuous loop families along A–B in **Figure 12b**. The bottom line of punch heads is common among them; the printed regions of die is uniformly removed by the sandblasting. The punch heads have homogeneously the height of 70 μm and the width of 60 μm, respectively.

### 3.4 Fine coining into copper substrate using the 3D-printed punch

The multi-head punch in **Figure 12a** was utilized for micro-embossing of the copper substrate plate with the size of 22 mm x 12 mm x 1 t mm. The CNC (computer numerical control) stamping system (ZEN; Hoden-Seimitsu, Yokohama, Japan) was used for this precise embossing. **Figure 13a** depicts the embossed copper plate with microgrooves. As compared between **Figures 12b** and **13b**, this microgroove texture is just corresponding to the multi-head pattern in the punch. The average microgroove depth is 50 μm and its width is 60 μm. Since its profile is transcribed by embossing the multi-head configuration in **Figure 12b**, its side walls are steeply formed against the substrate surface. This steep microgrooving configuration has influence on the robustness in mechanical joining between the plastic mold and the copper substrate.

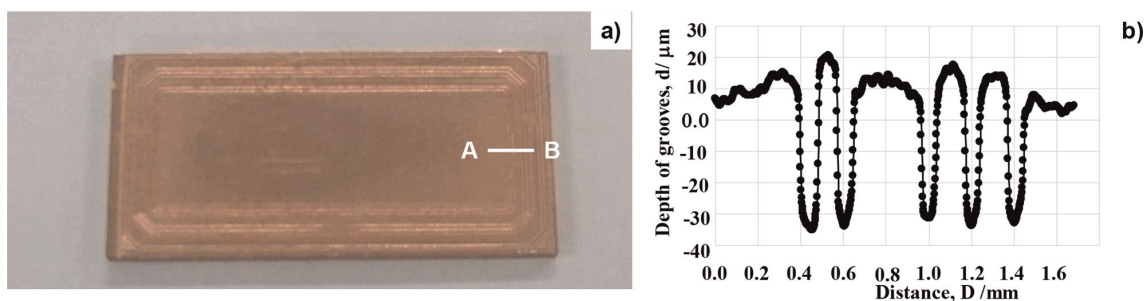


**Figure 13.** A pure copper plate embossed by using the plasma-printed punch. a) Overview of the embossed copper plate, and b) its cross-sectional profile along A–B.

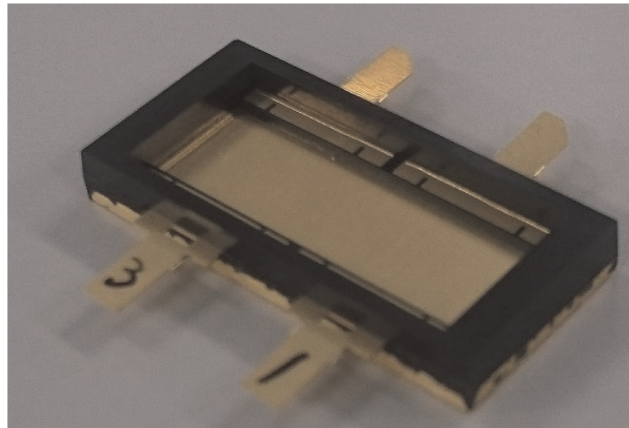


**Figure 14.**  
*A plastic mold package with joining the copper substrate plate through the microgrooves.*

### 3.5 Evaluation on the mechanical integrity of joined package

Twelve package specimens were prepared to evaluate their mechanical integrity by thermal transient loading and reflow testing. This testing procedure consists of three steps: 1) baking test at 398 K (or 125°C) for 24 h, 2) humidity test at 273 K (or 0°C) at 60% RH for 192 h, and 3) reflow testing at 533 K (or 260°C) for three cycles. A typical package specimen was depicted in **Figure 14**. The terminals were also housed into the specimen.

No leaks were noticed among 12 specimens; this demonstrated that perfect tightness can be accommodated to this packaging by using the 3D-printed microgrooves onto the copper substrate. Let us evaluate on the cost-competitiveness to the present manufacturing. In the normal laser processing, the CAM (computer-aided manufacturing) data must be built up before laser machining; this time reaches 36 ks for calculation of paths, editing the data and checking them. Excluding the setup time for laser path control, the actual processing time is accounted to be 150 s per each machining step. In the present procedure, the screen printing time to die surface is 300 s, the plasma nitriding processing time including the heating and cooling durations is 18.0 ks, and the sandblasting time is 300 s. The coining process by stamping requires 10 s per a copper substrate. The total setup time for laser machining is reduced in half by the present 3D printing. The actual laser machining time is shortened by 1/15. Consider that  $N$  copper substrates are processed to compare the real processing duration between two. In the normal laser machining, the duration is estimated by  $150 \times N$  s. On the other hand, the punch in **Figure 12a** is prepared to have  $N$  modules without excessive increase in the same manner as shown in the above. The total duration is nearly the same as 10 s. That is, the cost-competitiveness to the present procedure for multi-substrate fabrication is enhanced by  $15 \times N$ .

### 4. 3D printing of complex-shaped punch for piercing

The micro-parts and micro-tools must have functional geometries in their inside [34]. **Figure 15** depicts the CAD data of micro-valve to push up the liquid matter by the circular pendulum with three U-shaped springs. In particular, this U-shaped spring has accurate dimensions to satisfy the tailored elastic stiffness. The plasma nitriding-assisted 3D printing was utilized to build up the complex-shaped punch to

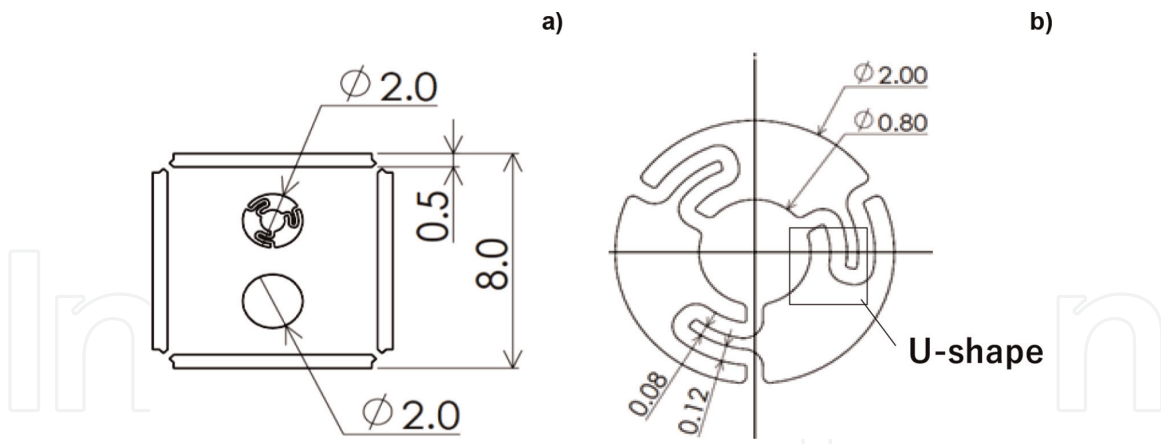


**Figure 15.** A micro-valve design as a unit functional sheet of micro-pump. a) AISI304 sheet with a through-hole and a valve section, and b) detail structure of micro-valve unit.

yield this valve sheet [35, 36]. This piercing punch was shaped after the general procedure in the Section 2. The core-die was directly shaved by using the hardened punch head into the die substrate. The mechanical finishing step was utilized to build up the narrow clearance between the 3D-printed punch and its shaved core-die. This pair of 3D-printed punch and shaved core-die was utilized for piercing the AISI304 sheet with the thickness of 0.05 mm to accommodate the micro-valve into the sheet in corresponding to CAD data as shown in **Figure 15** [37].

#### 4.1 Plasma printing of piercing punch

The plasma nitriding-assisted 3D printing procedure to fabricate the piercing punch was illustrated in **Figure 16**. The inkjet printing was utilized to draw the CAD data of micro-valve geometry onto the AISI316 punch surface as shown in **Figure 16a**. This punch was plasma-nitrided to selectively nitride the unprinted punch surfaces as shown in **Figure 16b**. The nitrided punch was sandblasted to remove the printed parts mechanically and to make near-net shaping of punch head as shown in **Figure 16c**. After the schematic steps in **Figure 16**, the inkjet printer (Mimaki, Tokyo, Japan) was utilized to draw the two-dimensional pattern onto the punch surface as depicted in **Figure 17a** in correspondence to **Figure 16a**. This printed punch was subjected to the plasma nitriding process to harden selectively the unprinted surfaces as shown in **Figure 17b**, corresponding to **Figure 16b**. The sandblasting was further employed to remove mechanically the soft parts. **Figure 17c** reveals that the complex-shaped punch heads are formed in fairly good reproduction of CAD data as shown in **Figure 16c**.

#### 4.2 Fine piercing of AISI304 sheets

The plasma-printed punch and the shaved core-die were utilized to punch out the AISI304 stainless steel sheet with the thickness of 50  $\mu\text{m}$ . CNC stamping system (Komatsu-Seiki-Kosakusho, Nagano, Japan) was employed in this punching process. **Figure 18** depicts the SEM image on the pierced micro-valve unit into the AISI304 stainless steel sheet. Comparing this with the CAD data in **Figure 16a**, the micro-valve unit is fabricated in exclusively negative to the CAD data for punch head in

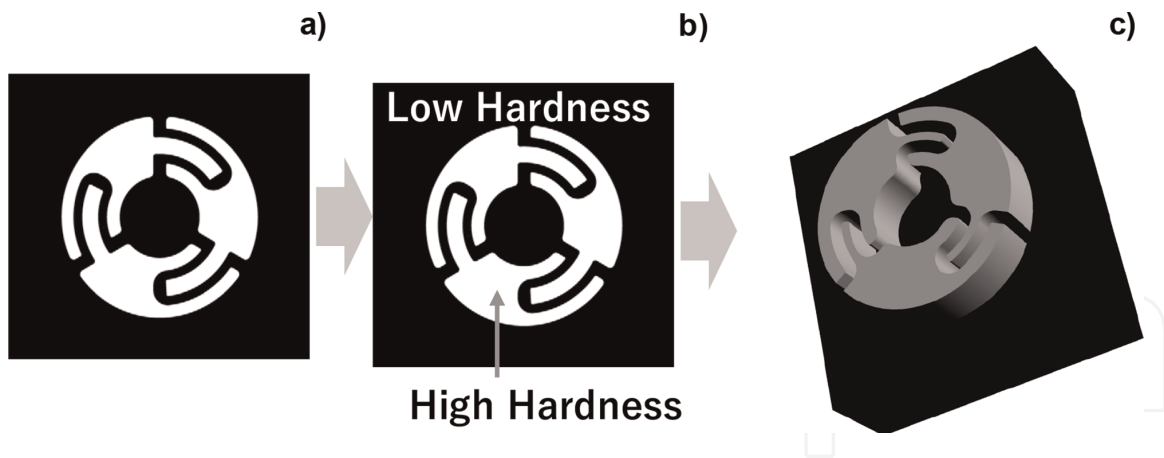


**Figure 16.** Plasma nitriding-assisted 3D printing scheme to fabricate the piercing punch. a) Inkjet printing step onto the punch top surface, b) low-temperature plasma nitriding step, and c) sandblasting step.

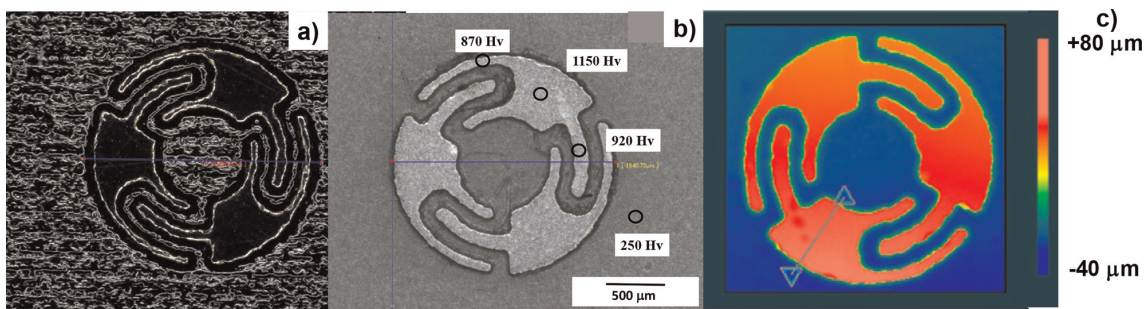


**Figure 17.** Plasma nitriding-assisted 3D printing procedure to fabricate the piercing punch. a) Inkjet printing, b) plasma nitriding, and c) sandblasting.

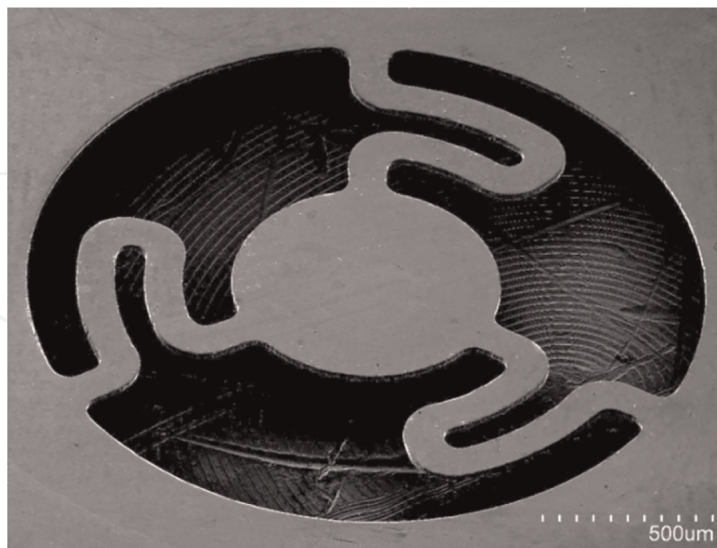


**Figure 18.** AISI304 stainless steel sheet with a micro-valve.

**Figure 16a.** This assures the dimensional accuracy of this plasma nitriding-assisted 3D printing to accommodate the functional units into the metallic sheets or films. To be noticed, a set of functional units can be punched out by using this 3D-printed punch with the shaved die.

## 5. 3D printing of complex-shaped dies for punching

Let us develop the other way to simultaneously fabricate a pair of punch and core-die for precise punching. Various mechanical parts have two-dimensional product shape such as the spur gears and wheels, the metallic belts, and the motor cores. In particular, a motor core consists of complex-shaped electrical steel sheets as a two-dimensional product. Then, each sheet has to be accurately punched out by stamping or forging [38]. The final motor core shape is controllable by joining or laminating the same constituent blanked sheets [39]. The plasma nitriding-assisted 3D printing is advanced to simultaneously fabricate the punch and core-die to punch out the fine blanked electrical steel sheets with sufficient accuracy in dimension [40].

### 5.1 Simultaneous plasma printing of punch and die

Every step starts from the same CAD data of product shape. In the present section, the CAD data for the T-shaped electrical steel sheet unit in **Figure 19a** is common to the whole steps in the plasma nitriding-assisted 3D printing process. In the procedure to fabricate the punch, the negative pattern to these original data was screen-printed onto the AISI316 substrate. On the other hand, the positive pattern was also screen-printed onto the substrate for fabrication of a core-die, as depicted in **Figure 19b**. In the subsequent plasma nitriding and sandblasting steps, both printed substrates were subjected to the same treatment. The T-unprinted part is selectively nitrided, and other parts are automatically removed from die substrate as depicted in **Figure 19c** and **d**. The piercing punch with the T-shaped head is fabricated by this 3D printing. While, other die substrates than T-printed part is selectively nitrided so that T-shaped part is automatically removed from die substrate also in **Figure 19c** and **d**. Then, the piercing core-die with the T-shaped cavity is fabricated by this 3D printing. To be discussed later, the clearance between the 3D-printed punch and core-die is determined by the dimensional tolerance in CAD data.

### 5.2 Plasma nitriding-assisted 3D printing of AISI316 punch and core-die

After the schematic procedure in **Figure 19**, AISI316 punch and core-die are simultaneously fabricated to demonstrate that a pair of special tools for fine stamping and forging is automatically yielded from the original CAD data.

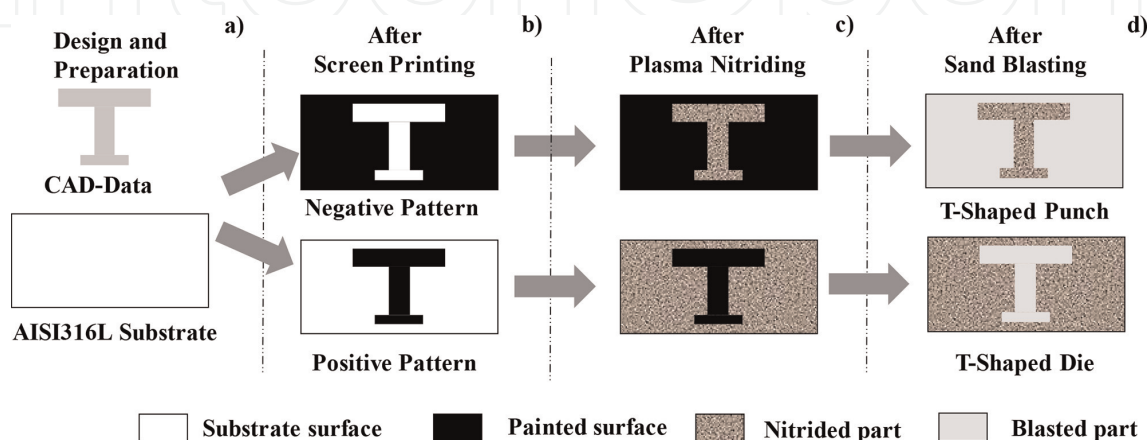


**Figure 19.** Simultaneous plasma nitriding-assisted 3D printing procedure to fabricate the piercing punch and core-die.

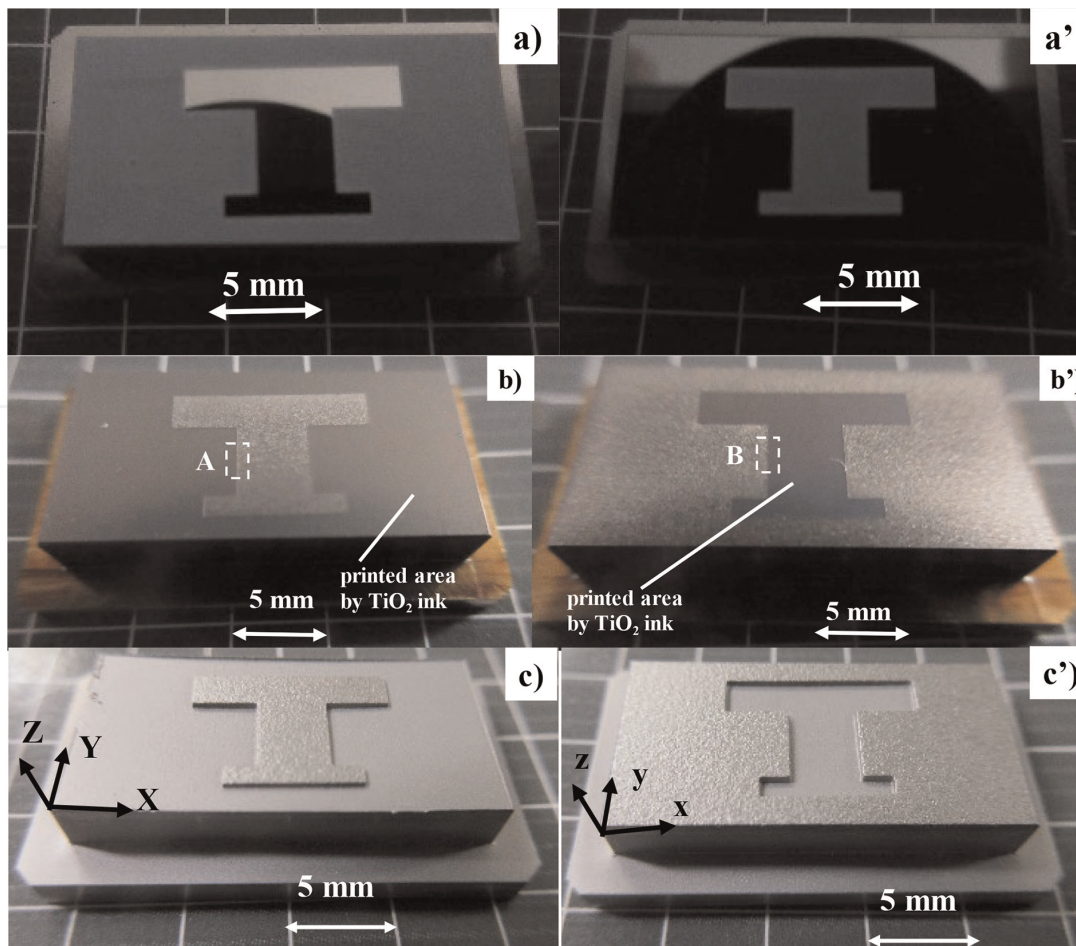


**Figure 20.**  
*Comparison of the plasma nitriding-assisted 3D printing procedures to simultaneously fabricate the T-shaped AISI316 punch and the T-shaped AISI316 core-die.*

In corresponding to the screen-printing step in **Figure 19b**, the negative region to T-shaped model is all printed in **Figure 20a**, and the T-shaped region is only printed onto the substrate surface in **Figure 20a'**. Both AISI316 substrates are plasma-nitrided together at 673 K for 14.4 ks. The unprinted T-shaped surface is selectively nitrided in **Figure 20b**, while the printed T-shaped surface is selectively un-nitrided in **Figure 20b'**. Both nitrided AISI316 substrates are sandblasted to remove the softer parts of substrates than the hardness of shooting media. As shown in **Figure 20c**, other parts of substrate than T-shaped region are removed to leave the T-shaped punch head. On the other hand, the T-shaped region is exclusively dug and removed from the substrate to leave the T-shaped die cavity as depicted in **Figure 20c'**.

Three-dimensional profilometer was utilized to measure the T-shaped head of punch in **Figure 20c** and the T-shaped cavity of core-die in **Figure 20c'**. As shown in **Figure 21a**, the T-shaped head has uniform height of 350  $\mu\text{m}$  and other surface is homogeneously ground by the present 3D printing. That is, the AISI316 punch is fabricated after the printing scheme in **Figure 19** to have a T-shaped head with uniform height. On the other hand, the T-shaped cavity is uniformly dug by 350  $\mu\text{m}$  in depth; the cavity walls have steep gradient against the die surface in **Figure 21b**. AISI316 core-die is fabricated to have a T-shaped cavity with the uniform depth in correspondence to the T-shaped punch.



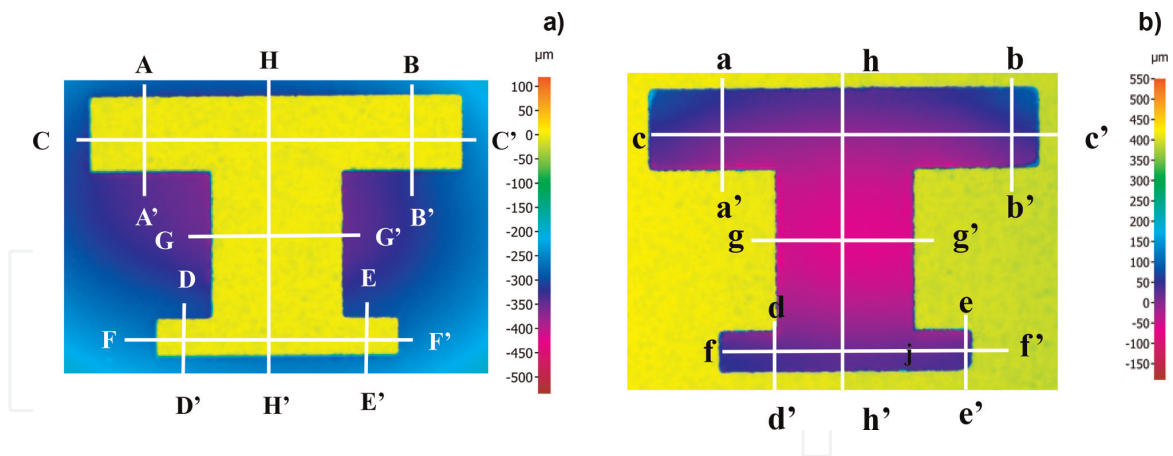


**Figure 21.** Comparison of three-dimensional profile between the T-shaped punch head and the T-shaped core-die cavity.

Among several cross sections from A-A' to F-F' in **Figure 21a** and from a-a' to f-f' in **Figure 21b**, the cross sections of F-F' and f-f' were selected to describe the three-dimensional profile of T-shaped punch head and die cavity.

As compared in **Figure 22**, the T-shaped punch head and die cavity has uniform height of 350 µm and uniform depth of 350 µm with small roughness. The punch head and die cavity side surfaces are steeply formed to be perpendicular to the punch head and cavity bottom surfaces, respectively. The punch edge width and die cavity edge width are 15 µm and 20 µm, respectively. These dull edges influence on the shearing process in piercing process.

The clearance between the punch head and die cavity is an essential parameter with significant influence on the product quality through stamping and forging and on the shearing behavior [41]. In the present 3D printing, no tolerance for clearance control was performed in CAD; the effective clearance is autonomously determined by the accuracy in the plasma printing steps. Let us describe the allowable clearance by three-dimensional profiling on the cross sections along A-A' to F-F' and a-a' to f-f'.

**Table 1** compares the original CAD data on the edge lengths with the measured T-shaped punch and core-die dimensions along A-A' to F-F' in **Figure 20a** and a-a' to f-f' in **Figure 20b**, respectively. In the plasma printing step of T-shaped punch, the dimensional deviation per the punch edge length ranges from - 3% to +0.2%. This printing of punch accompanies with negative tolerance. On the other hand, the edge length of T-shaped core-die deviates from +0.5% to +5% per the core edge length. The printing of core-die accompanies with positive tolerance. Hence, the clearance is

	A-A' a-a'	B-B' b-b'	C-C' c-c'	D-D' d-d'	E-E' e-e'	F-F' f-f'	G-G' g-g'	H-H' h-h'
Screen (mm)	2.0	2.0	10.0	1.0	1.0	6.5	3.5	7.0
T-letter punch (mm)	2.001	1.991	10.001	0.978	0.971	6.512	3.476	6.990
T-letter core-die (mm)	2.023	2.039	10.045	1.047	1.039	6.531	3.561	7.073
Clearance (mm)	0.011	0.024	0.022	0.034	0.035	0.0095	0.043	0.0415

**Table 1.** Comparison of the geometric accuracy among the CAD data, the measured T-shaped punch, and core-die dimensions and the calculated clearances.

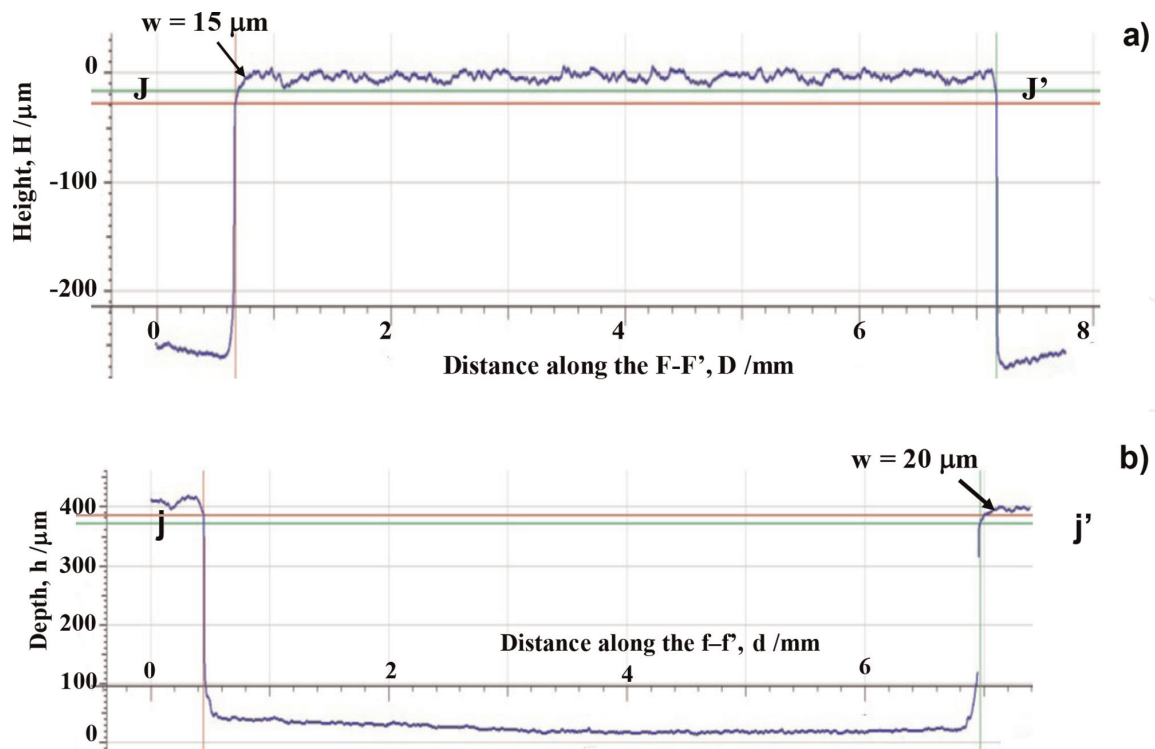


**Figure 22.**  
Comparison of the three-dimensional profiles between the T-shaped punch head and die cavity at the cross section along F-F' in Figure 21a and f-f' in Figure 21b.

determined by the sum of two tolerances; the maximum clearance reaches +3.5% in Table 1.

### 5.3 Fine punching of electrical steel core unit sheets

The CNC stamping system (Precise Metal Forming Laboratory; Hachi-Oji, Japan) was utilized for punching out the electrical steel sheet with the thickness of 200  $\mu\text{m}$  by using this T-shaped punch and die pair. Figure 23 depicts the pierced electrical steel core sheet and its skeleton. No distortion was observed on both sheets; this pair is useful in continuous punching operations for mass production. As shown in Figure 24, the burnished cross-sectional surface area reaches 70% just in correspondence to highly qualified sheared surface with much lower clearance in [38].

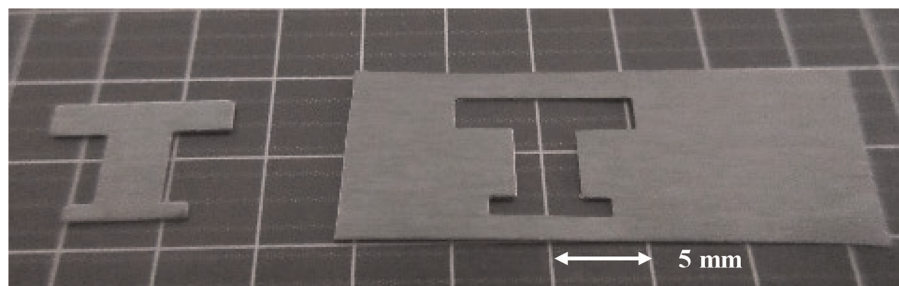


**Figure 23.**  
The pierced electrical steel core unit and its skeleton.

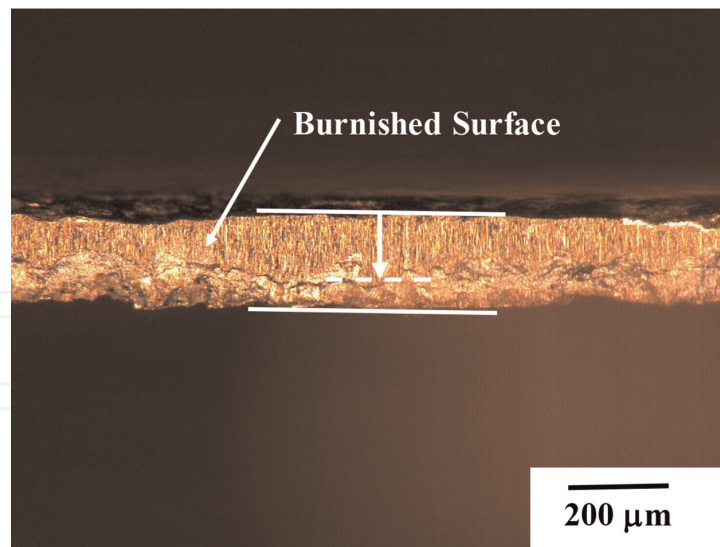


**Figure 24.** SEM image on the sheared surface of pierced electrical steel sheets along F-F' in Table 1.

## 6. Production line for fabrication of micro-pumps with aid of 3D printing

Most of medical tools and devices must have sufficient durability to be free from damage and risk of failure [42]. A micro-pump has to equip the sufficient leak proof against the pressurized blood, the drug solution, the liquid food, and so forth, never to splash them even into the human body [43, 44]. In addition to the original strength and toughness of its constituent materials, it has sufficiently high joining strength among these constituent units and parts.

In this section, the mother AISI304 sheet with the thickness of 50  $\mu\text{m}$  is punched out by using each plasma-printed punch and die pair to fabricate each constituent sheet unit with the accommodated function [45]. Several to ten sheet units are assembled and joined to a micro-pump. The punching process of constituent sheet units and their assembling and joining processes work in parallel as a production line [46] as illustrated in Figure 1.

### 6.1 Production line design for fabrication of micro-pump

A production line was designed and developed after the scheme in Figure 1 to make 3D printing of the micro-pump from the AISI304 austenitic stainless steel sheets as a feedstock. A whole procedure is shown in Figure 25. This system mainly consists of two subsystems. The sliced 2D CAD data from the original product 3D model of micro-pump unit is transformed into the punch head and die cavity by the plasma nitriding-assisted 3D printing. Each plasma-printed punch and die is utilized in blanking, embossing, piercing, and punching the AISI304 sheet with the tailored thickness. The assembly of the blanked, embossed, and punched-out sheets, is polished and cleaned by the argon and hydrogen plasmas. Through the bombardment by argon ions and the chemical reduction by activated hydrogen atoms, the thickness of passive oxide film on the work surfaces is reduced or removed to lower the joining temperature. Under the inert atmosphere, the cleaned and polished assembly is stacked into a preform with laminated work sheets and joined by hot stamping with

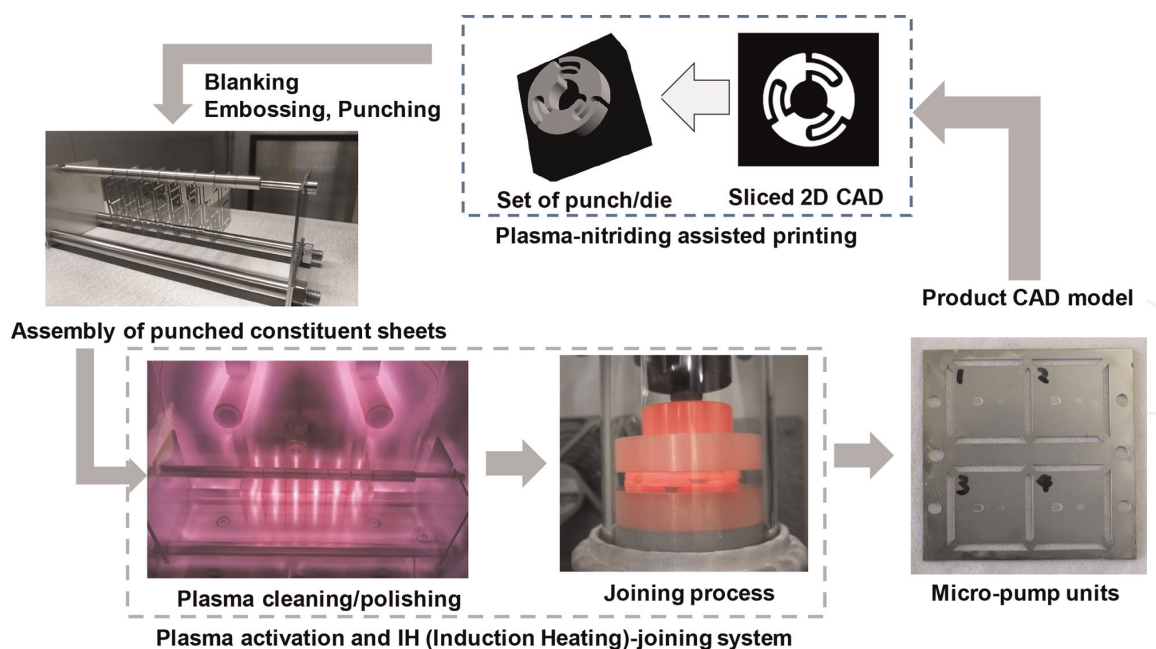


**Figure 25.**  
 Production line for micro-manufacturing of micro-pump from the feedstock of AISI304 sheets.

the use of high-frequency induction heating (HFIH) units. Four micro-pump units are produced by this procedure in a single shot.

In the same manner as explained in the sections 4 and 5, the finished set of punch and die is utilized to blank, emboss, pierce, and punch out the AISI304 sheet with the selected thickness from 200  $\mu\text{m}$  to 10  $\mu\text{m}$ , respectively. The shaped sheet is set as an assembly and transferred to the plasma activation and HFIH joining system.

## 6.2 Plasma polishing and cleansing of AISI304 sheet unit assembly

The normal hot-pressing in the nitrogen or argon atmosphere was effective to join the stacked sheets. However, the joining performance is completely governed by the separation of oxide layer through the oxygen atom diffusion into the matrix [47]. Since the onset temperature of oxide layer separation is around 1223 K (or 950°C), the joining temperature is estimated to be 1250 K. This holding temperature in hot pressing is possible to induce the thermal distortion to disturb the dimensional accuracy and the damage to stainless steels. Hence, the pretreatment before joining is needed to reduce the oxide layer thickness and to lower the holding temperature for joining.

In the present study, the argon and hydrogen plasma activation process was utilized to clean and polish the top and bottom surfaces of constituent sheets in the assembly. As shown in **Figure 25**, the oxide layer thickness was reduced by the bombardment of argon ions and the chemical reduction reaction via  $\text{MO}_x + 2\text{H} \rightarrow \text{M} + x\text{H}_2\text{O}$  (M: Fe or Cr) in the plasma sheath. **Figure 26** compares the variation of peeling strength with increasing the holding temperature for joined specimens with and without the plasma surface activation.

At  $T_H = 1043 \text{ K}$  (or 770°C), the peeling strength of joined specimens with plasma activation becomes nine times higher than that without plasma activation. This proves that the passive oxide layer thickness of AISI304 stainless steel sheets is reduced enough to significantly improve the joining strength.

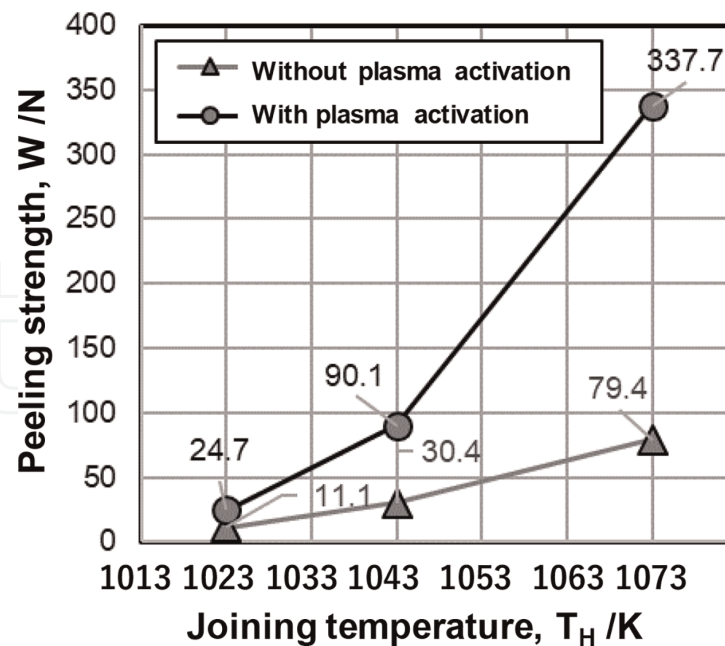


**Figure 26.**

Variation of the peeling strength ( $W$ ) with increasing the joining temperature ( $T_H$ ) for the joined specimens at 30 MPa for 1.8 ks with and without plasma activation in the plasma polishing and cleansing process.

### 6.3 Low-temperature joining of assembly to micro-pump part

The sufficient joinability is essential to certify the proof of mechanical integrity for a micro-pump in practical operation [48]. The higher peeling strength than 100 N is a necessary condition for this integrity proof as an essential mechanical engineering item. In addition, the fractography [49] on the peeled interfaces between the stainless steel sheets provides a material science tool to validate the sufficient joinability. In general, the brittle fractured surface is characterized by the smooth surfaces with little micro-voids [50]. On the other hand, the ductile fractured surface consists of the micro-dimples and micro-voids [51]. Hence, the integrity of joined surface is investigated by the fractography on the peeled surface. **Figure 27** compares the SEM image on the cross section of joined specimens at 1073 K for 1.8 ks by 30 MPa with and without plasma activation as well as their fractography. In the joined specimen without plasma activation, the boundary between the joined sheets is distinguished by each granular micro-structure. The peeled-out interface is flat including little micro-voids. While, in the joined specimen with plasma activation, the recrystallized grains are seen on the sheet boundary. Two adjacent stainless steels are joined to form new grains across the previous interface boundaries. The whole peeled-out surface consists of the micro-dimples and micro-voids. They were formed by the ductile fracture during the peeling test. This difference assures the high joinability on the interfaces of stainless steel assembly.

## 7. Discussion

The present plasma nitriding-assisted 3D printing has three merits superior to the traditional die technologies by mechanical milling [52] and laser machining [53]. As seen in comparison between the CAD data and the punch head and die cavity in **Figures 11**, **17**, and **20**, their geometric configuration is just corresponding to the CAD data. This assures that any punch and die can be fabricated through the duplication of two-

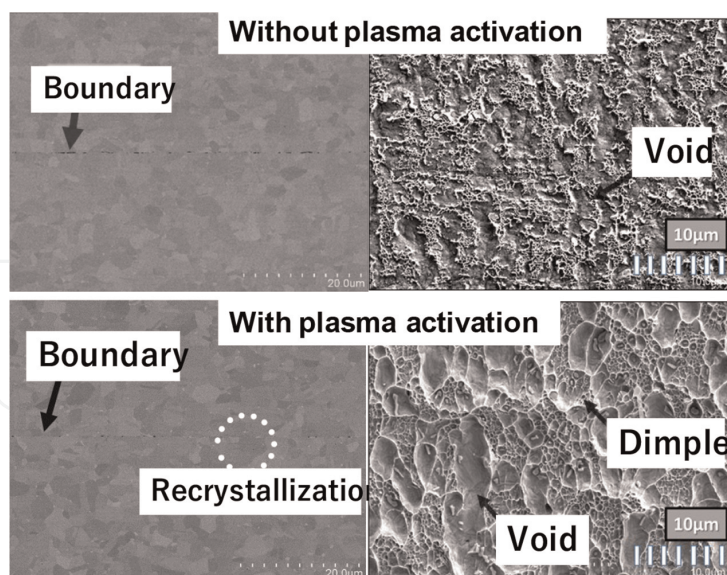


**Figure 27.** Comparison of the SEM image on the microstructure of joined interface in low and high magnifications between the joined specimens at 1073 K by 30 MPa for 1.8 ks with and without plasma activation.

dimensional CAD in the present approach. In particular, the clearance between the punch head and die cavity is autonomously determined by the present plasma printing. This first merit is effective to build up the complex-shaped punch and die as well as the multi-head punch and multi-cavity die for mass production of mechanical parts [54].

Higher hardness than 800 HV in the plasma-printed punch and die substrates becomes the second merit for die technology. Since the lower hardness parts are removed by sandblasting, the punch head and die surface are proved to have much higher hardness than their mother substrate materials by plasma nitriding. Various stainless steels and tool steels are available as an original substrate material for this plasma printing [55].

The autonomous formation of steep side surfaces in the punch and die turns to be the third merit to prepare a die pair for embossing, piercing, and punching processes as shown in **Figures 12, 17, 21, and 22**. In particular, this merit works well in fabrication of sub-mm and sub-100  $\mu\text{m}$ -sized products by stamping with the use of plasma-printed punch and die pair [56]. As noticed in **Figures 22 and 25**, the punch and die edges must be sharpened to improve the shearing behavior in embossing, piercing, and punching processes. At first, the plasma-printed punch and die might well be ground to reduce their edge widths of 15–20  $\mu\text{m}$  down to a few  $\mu\text{m}$ . Then, an ion milling is employed to finish the edge width down to 1  $\mu\text{m}$  or less than. As reported in [57, 58], the edge-sharpened punch and die with higher hardness than 1000 HV by the plasma nitriding has a capacity to improve the quality of sheared surfaces without loss of die life.

In the present 3D printing method, its dimensional accuracy of products is first determined by the spatial resolution ( $D$ ) in drawing the 2D micro-pattern onto the die substrates. As depicted in **Figure 2**, the metal masking, the inkjet, and screen printing are only available to micro-patterning with  $D > 10 \mu\text{m}$ . When aiming at fine resolution for  $D < 10 \mu\text{m}$ , the lithography and the laser masking techniques are only available in this method. As reported in [59, 60], the normal maskless lithography was used to prepare the complex-shaped micro-patterns by  $D = 0.5 \mu\text{m}$  for plasma-printing the multi-head DLC (Diamond-Like Carbon) punches and the micro-nozzles. In order to improve the spatial resolution toward  $D \ll 1 \mu\text{m}$ , these two methods must be advanced together with suitable selection of inks, resins, and metallic deposits.

Owing to the principle of plasma nitriding assistance in this 3D printing, the whole surfaces of punch head and die cavity are hardened and enriched by nitrogen solutes in high content. After [61, 62], they have sufficient wear resistivity and corrosion roughness to be working in long-term usage of mass production. In addition to the titanium and titanium alloy sheets with high chemical affinity to die substrate materials [63], the thermoplastic plastic sheets are embossed, pieced, and punched to the constituent element of micro-parts by using the plasma-printed dies [64].

In the additive sheet manufacturing, the low-temperature joining process plays an essential role to reproduce the tailored micro-pump unit after the 3D CAD model with sufficient integrity proof. High interfacial strength by ductile joining among the sheet interfaces assures the leak proof to be working at the specified operation conditions for the designed product life. When this proof standard is relaxed, other joining methods are also available in the present additive sheet manufacturing. Among them, the mechanical clinching method [65] provides the elasto-plastic interlocking between adjacent sheets with sufficient interfacial strength. This pointwise joining has no rooms of leak proof against the fluids and solutions. The mechanical anchoring method [66] also becomes a suitable joining of dissimilar plastic sheets into a product with sufficient strength and water proof in addition to the joining of plastic mold with the metallic substrate in the Section 3.

A micro-pump was produced in two-step procedure. At first, its constituent stainless steel sheets are punched out by using the plasma-printed punch and die in correspondence to the 2D sliced data of its 3D model. In second, these punched-out sheets are assembled, plasma-cleaned and polished, and HFIH-joined to yield the four micro-pump units. Most of MEMS units are produced in the same manner. In particular, the pendulum in the micro-valve in **Figure 18** has no risk of local distortion and no hot adhesion to other sheet parts in wrong. This allows us to design various inner spaces for device movement in the MEMS.

The micro-inspection units [67] are a typical micro-part, working in vitro. They consist of several functional subunits including the micro-fluidic unit to control the chemical reaction rates for inspection, the micro-reservoir unit to control the pressure in the micro-channel flow, and so forth. Each subunit consists of two or three AIS304 stainless sheets shaped by the present printing process. The micro-injectors [68] embedded in vivo into deceased parts of body are also fabricated by the present 3D printing for local drug delivery and for curing the local tissue.

## **8. Conclusion**

The plasma nitriding-assisted 3D printing was proposed to fabricate the complex-shaped punch and die for fine embossing, piercing, and punching processes and to yield the functionalized constituent sheets by using the CNC stamping. Through the embossing process, the tailored microgroove array is accommodated to the copper substrate for mechanical anchoring of the plastic molds in the leak-proof packaging. Through the piercing process, the micro-valve unit is housed into the stainless steel sheet for functionalization of sliced 2D CAD data from 3D solid model of micro-pump. The electrical steel sheets are punched out to yield the T-shaped motor core units for assembly to a motor core by mechanical joining or mechanical anchoring. These sheet elements with functional units for sliced 2D model are plasma-cleaned and polished and joined at low temperature to build up the micro-pump unit in correspondence to the original product model.

The design flexibility is preserved by transformation of the 2D CAD data to the constituent metal or polymer sheet through the embossing, piercing, and punching processes with the use of plasma-printed punch and die. The hot stamping, as well as the mechanical joining, is useful to integrate the discrete functionalized sheets into a continuous micro-element and part. This 3D printing with the use of metal and polymer films, sheets and plates as a feedstock, provides a new way of additive micro-manufacturing to yield the MEMS units with high mechanical integrity and the medical tools to be working in vitro and in vivo.

## **Acknowledgements**

The authors would like to express their gratitude to Kurozumi S-I. and Morita H. (Nano-Film Coat, llc.), Yoshino T. (Komatsu-Seiki Kosakusho, Co., Ltd.), and graduate students both in the Shibaura Institute of Technology and the University of Toyama for their help in experiments. This study was financially supported in part by the Grand-In-Aid from METI, Japan.

## **Conflict of interest**

The authors declare no conflict of interest.

## **Abbreviations**

CAD	Computer-Aided Design
CAM	Computer-Aided Machining
CNC	Computer Numerical Control
DC	Direct Current
EDX	Energy-Dispersive X-ray spectroscopy
GaN	Gallium Nitride
PZT	Lead (Pb) Zirconate Titanate
RF	Radio Frequency
SEM	Scanning Electron Microscopy
2D	Two Dimension
3D	Three Dimension



IntechOpen

### **Author details**

Tatsuhiko Aizawa<sup>1\*</sup>, Tomomi Shiratori<sup>2</sup> and Yohei Suzuki<sup>3</sup>

1 Surface Engineering Design Laboratory, Shibaura Institute of Technology, Tokyo, Japan


2 Faculty of Engineering, University of Toyama, Toyama, Japan

3 Komatsu-Seiki Kosakusho, Co., Ltd., Suwa, Japan

\*Address all correspondence to: taizawa@sic.shibaura-it.ac.jp

### **IntechOpen**

---

© 2022 The Author(s). Licensee IntechOpen. This chapter is distributed under the terms of the Creative Commons Attribution License (<http://creativecommons.org/licenses/by/3.0>), which permits unrestricted use, distribution, and reproduction in any medium, provided the original work is properly cited. 

## References

- [1] Kumar SA, Prasad RVS, Basic principles of additive manufacturing: different additive manufacturing technologies. In: Additive Manufacturing Woodhead Pub. Ch. 2. 2021. pp. 17-35
- [2] ISO/TC 261 additive manufacturing, ISO.ASTM 52907:2019 Additive manufacturing feedstock materials – methods to characterize the metal powders. 2019. pp. 1-19
- [3] Munsch M, Laser additive manufacturing of customized prosthetics and implant- feedstock amts for biomedical applications. In: Laser Additive Manufacturing – Materials, Design, Technologies and Applications – Woodhead Pub. Ch. 15. 2017. pp. 399-420
- [4] Zhong Y, Raenner L-E, Lie L, Koptyung A, Wikman S, Olsen J, et al. Additive manufacturing of 316L stainless steel by electron beam melting for nuclear fusion applications. *Journal of Nuclear Materials*. 2017;**486**:234-245
- [5] Alberti EA, Bueno BMP, D'Oliveira ASCM. Additive manufacturing using plasma transferred arc. *The International Journal of Advanced Manufacturing Technology*. 2016;**83**:1861-1871
- [6] Loterie D, Derrot P, Moser C. High-resolution tomographic volumetric additive manufacturing. *Nature Communications*. 2020;**11**:852-861
- [7] Zhang J, Jung YG, editors. Additive Manufacturing –Materials, Processes, Qualifications and Applications. London, UK: Elsevier; 2018
- [8] Shiratori T, Nakano S, Suzuki Y, Katoh M, Sato N, Komatsu T, et al. Development of metal MEMS manufacturing technologies using pierced metal foil and diffusion bonding process at low temperature. In: Proc. 4M/IWMMF2016 Conference. Copenhagen, Denmark: 4M Conf. Committee; 2016. pp. 209-212
- [9] Arnold J. *Die Makers Handbook*. 1st ed. Cumberland, USA: Industry Press; 2020
- [10] Katoh T, Aizawa T, Yamaguchi T. Plasma assisted nitriding for micro-texturing onto martensitic stainless steels. *Manufacturing Review*. 2015;**2**(2): 1-7
- [11] Aizawa T, Redationo NT, Mizushima K. Precise micro-texturing onto DLC coating via high density oxygen plasma etching. *Proceedings of 4M-Conference*. 2013;**1**:129-132
- [12] Aizawa T, Yamaguchi T. High-density plasma nitriding assisted micro-texturing onto martensitic stainless steel mold-die. *Proceedings of 9th IWFM*. 2014;**2A**:11-f7
- [13] Aizawa T, Wasa K. Fine micro-fabrication of stainless steel nozzle array by plasma printing. *Proceedings of WCMNM-2018*. 2018;**1**:65-68
- [14] Aizawa T, Tamaki M, Fukuda T. Motion-controlled CNC stamping for micro-texturing onto metallic sheet. *Proceedings of 9th ICOMM*. 2014;**14**:1-8
- [15] Aizawa T, Inohara T. Micro-texturing onto glassy carbon substrates by multi-axially controlled pico-second laser machining. *Proceedings of 7th ICOMM*. 2012;**1**:66-73
- [16] Aizawa T, Shiratori T, Saito Y. Fabrication of micro-punch array by

plasma printing for micro-embossing into copper substrates. Proceedings of 12th AWMFT. 2019;1:93-98

[17] Shiratori T, Aizawa T, Saito Y, Wasa K. Plasma printing of an AISI316 micro-meshing punch array for micro-embossing onto copper plates. *Journal of Metals*. 2029;9(396):1-11

[18] Aizawa T, Sugita Y. High density RF-DC plasma nitriding of steels for die and mold technologies. *Research Reports SIT*. 2013;57(1):1-10

[19] Aizawa T, Sugita Y. High density plasma nitriding of tool and die steels. Proceedings of 6th SEATUC Symposium. 2012;1:134-137

[20] Kuwahara H. Fundamentals and Application of DC-Plasma Nitriding and Carburizing. PhD Thesis. Kyoto, Japan: Kyoto University; 1992

[21] Hiraoka Y, Inoue K. Prediction of nitrogen distribution in steels after plasma nitriding. *Denki-Seiko*. 2010;86:15-24

[22] Granito N, Kuwahara H, Aizawa T. Normal and abnormal microstructure of plasma nitrided Fe-Cr alloys. *Journal of Materials Science*. 2002;37(4):835-844

[23] Farghali A, Aizawa T. Phase transformation induced by high nitrogen content solid solution in the martensitic stainless steels. *Materials Transactions*. 2017;58:697-700

[24] Farghali A, Aizawa T. Nitrogen supersaturation process in the AISI420 martensitic stainless steels by low temperature plasma nitriding. *ISIJ International*. 2018;58(3):401-407

[25] Aizawa T. Low temperature plasma nitriding of austenitic stainless steels. In:

*Stainless Steels*. London, UK: IntechOpen; 2018. pp. 31-50

[26] Aizawa T, Yoshihara S-I. Inner nitriding behavior and mechanism in stainless steels at 753 K and 623 K. *SEATUC Journal of Science and Engineering (SJSE)*. 2019;1:13-20

[27] Aizawa T, Shiratori T, Yoshino T, Suzuki Y, Komatsu T. Nitrogen supersaturation of AISI316 base stainless steels at 673 K and 623 K for hardening and microstructure control. In: *Stainless Steels*. Ch. 1 ed. London, UK: IntechOpen; 2021

[28] Aizawa T, Shiratori T, Saito Y. Fabrication of micro-punch array by plasma printing for micro-embossing into copper substrates. In: *Proc. 12th Asia Workshop on Metal Forming Technology*. Tokyo, Japan: JSTP; 2019. pp. 93-98

[29] Aizawa T., Shiratori T., Wasa K., Plasma-printed AISI316L multi-punch array for fabrication of aluminum heatsink with micro-pillar fins. Proceedings of 3rd WCMNM (Raleigh, USA) 2019;1: 220-223

[30] Aizawa T, Yoshihara S-I. Microtexturing into AISI420 dies for fine piercing of micropatterns into metallic sheets. *Journal of JSTP*. 2019;60(698): 53-57

[31] Saito Y, Aizawa T, Wasa K, Nogami Y. Leak-proof packaging for GaN chip with controlled thermal spreading and transients. Proceedings of 41st BCICTS2018. 2018;1:243-246

[32] Aizawa T, Saito Y, Hasegawa H, Wasa K. Fabrication of optimally micro-textured copper substrates by plasma printing for plastic mold packaging. *International Journal of Automation Technology*. 2020;14(2):200-207

- [33] Aizawa T, Nakata H, Nasu T, Nogami Y. Micro-textured graphitic substrate – Copper packaging for robustness. In: Proc. 5th WCMNM. Leuven, Belgium: Res. Pub.; 2022. pp. 291-295
- [34] Geiger M, Vollertsen F, Kals R. Fundamentals on the manufacturing of sheet metal microparts. *CIRP Annals*. 1996;**45**(19):277-282
- [35] Aizawa T, Takashima T, Shiratori T. Plasma printing to fabricate the micro-piercing dies for miniature metal products. In: Proc. 8th AWMFT. Suwa, Japan: CD-ROM; 2015
- [36] Aizawa T, Takashima T, Shiratori T, Suzuki Y. Fabrication of micro-piercing dies and punches via plasma printing. In: Proc. 11<sup>th</sup> ICOMM. Vol. 2. California, USA: I2M2; 2016. pp. 1-5
- [37] Shiratori T, Nakano S, Suzuki Y, Aihara T, Yang M. Development of multiple shape one process piercing method by laser processing punch. In: Proc. 2016 JSTP. Kyoto, Japan: JSTP; 2016. pp. 313-314
- [38] Katsuta E, Aizawa T, Morita H, Dohda K, Anzai M. Fine piercing of electromagnetic steel sheets by micro-punches under nearly zero clearance. *Procedia Manufacturing*. 2018;**15**:1459-1466
- [39] <https://www.emobility-engineering.com/motor-laminations/> [Accessed: October 15, 2022]
- [40] Aizawa T, Suzuki Y, Yoshino Y, Shiratori T. Fabrication of punch and die using plasma-assisted 3D printing technology for piercing sheet metals. *Journal of Manufacturing and Materials Processing*. 2022;**6**(49):1-15
- [41] Schmidt K. *Manufacturing Processes for Engineering Materials*. 5th ed. Hoboken, NJ, USA: Prentice Hall; 2008
- [42] Aizawa T, Satoh T, Shiratori T, Proc. 22nd Int. ESAFORM Conf. Mater. Form. AIP Conf. Proc. 2019;**2113**(050007):1-6
- [43] Satoh T, Aizawa T, Shiratori T, Sugita Y, Anzai M. Micro-joining of multi stainless steel sheets into mechanical element by low temperature diffusion process. *Procedia Manufacturing*. 2018;**15**:1475-1480
- [44] Satoh T, Aizawa T, Shiratori T, Yoshihara S-I. Micro-joining of multiple stainless-steel sheets into a mechanical element by low-temperature diffusion process. *J. JSTP*. 2019;**60**:80-84
- [45] Aizawa T, Shiratori T. Microforming of mechanical elements, devices and systems by additive sheet-manufacturing. *Proceedings of 12th AWMFT-2019*. 2019;**1**:1-6
- [46] Aizawa T, Shiratori T. Microforming of stainless steel miniature pump by additive sheet-manufacturing. *Materials Transactions*. 2020;**60**(2):266-271
- [47] Sugimoto K. Passive films on stainless steels – Present state of analysis and understanding. *Ziryo-to-Kankyo*. 2008;**57**:375-384
- [48] Kelly T, Childers RW, Busby D, Rodolfo Roger R, Sayyid WME, Din S. Medical fluid pump valve integrity test methods and systems. US-Patent. US9072831B2. 2004
- [49] Hayes MD, Edwards DB, Shah AR. *Fractography in Failure Analysis of Polymers*. London, UK: Elsevier; 2015
- [50] Quinn GD. *Fractography of brittle materials: Analysis of fractures in ceramics and glasses*. *Microscopy and Analysis*. 2008;**5**:21-24

- [51] Li H, Fu M. Deformation-Based Processing of Materials. London UK: Elsevier; 2019
- [52] Rahman M, Asad ANMA, Wang YS, Shinno H, Li X. Advanced machining technologies. In: Comprehensive Materials Processing. Vol. 11, London, UK: Elsevier; 2014
- [53] Aizawa T, Inohara T. Pico- and femtosecond laser micromachining for surface texturing. In: Stanimirovi'c Z, Stanimirovi'c I, editors. Chapter 1 in: Micromachining. London, UK: IntechOpen; 2019. pp. 1-23
- [54] Aizawa T, Morita H. Dry progressive stamping of copper-alloy snaps by the plasma nitrided punches. Materials Science Forum. 2018;**920**:28-33
- [55] Aizawa T, Shiratori T, Komatsu T. Micro-/nano-structuring in stainless steels by metal forming and materials processing. Chapter 5 In: Electron Crystallography. London, UK: IntechOpen; 2020. pp. 101-122
- [56] Pratap A, Patra K, Dyakonov M. Manufacturing miniature products by micro-grinding; a review. Procedia Engineering. London, UK: Elsevier; 2016;**150**:969-974
- [57] Aizawa T, Yoshino T, Shiratori T, Dohda K. Material characterization on the affected zones by fine piercing into single crystal Fe-6Si steel sheet. In: Proc. 4th WCMNM. Mumbai, India; 2021
- [58] Aizawa T, Shiratori T, Yoshino T, Suzuki Y, Dohda K. Quantitative characterization of the affected zones in a single crystal Fe-6Si steel sheet by fine piercing. Journal of Micromachines. 2022;**13**(562):1-15
- [59] Aizawa T. Micro-texturing onto amorphous carbon materials as a mold-die for micro-forming. Applied Mechanics and Materials. 2013;**289**:23-37
- [60] Aizawa T, Wasa K. Plasma printing of micro-nozzles with complex shaped outlets into stainless steel sheets. Journal of Micro-Nano-Manufacturing, ASME. 2019;**7**:034502/1-034502/6
- [61] Aizawa T, Fukuda T, Morita H. Low temperature high density plasma nitriding of stainless steel molds for stamping of oxide glasses. Manufacturing Review. 2016;**3**(5):1-6
- [62] Borgioli F, Galvanetto E, Bacco T. Low temperature nitriding of AISI300 and 200 series austenitic stainless steels. Vacuum. 2016;**12**:51-60
- [63] Aizawa T, Shiratori T. Plasma 3D-printing of micro-punch array for fine embossing into biomedical titanium works. Advances in Metallurgy Materials Engineering. 2020;**3**(1):95-103
- [64] Aizawa T, Yamaguchi T. Plasma nitriding assisted micro-texturing into martensitic stainless steel molds for injection molding. Proceedings of 10th 4M/ICOMM. 2015:454-459
- [65] Lambiase F, Ilio AD. Damage analysis in mechanical clinching; experimental and numerical study. Journal of Materials Processing Technology. 2016;**230**:109-120
- [66] Aizawa T, Satoh S, Yamaguchi T. Micro-texturing design for joining between polymer components. Proceedings of 9th ICOMM. 2014;**15**:1-8
- [67] Balouiri M, Sadiki M, Ibnsouda SK. Methods for in vitro evaluation antimicrobial activity: A review. Journal of Pharmaceutical Analysis. 2016;**6**(29):71-79
- [68] Henley T, Thomas K, Bressan M. Microinjection-based system for in vivo implantation of embryonic cardiomyocytes in the avian embryo. Journal of Visualized Experiments. 2019; **144**:e59267